26th ABCM International Congress of Mechanical Engineering
November 22-26, 2021. Florianópolis, SC, Brazil

COB-2021-0172
AN ALTERNATIVE APPROACH TO COMPUTE THE MATERIAL PARAMETERS FOR THE PERIDYNAMIC THEORY

Átila Lupim Cruz
Mechanical Division, Institute of Aeronautics and Space - IAE, Praça Marechal Eduardo Gomes, 50, Vila das Acácias, 12228-904, São José dos Campos, São Paulo, Brazil
atila.lc@hotmail.com

Mauricio Vicente Donadon
Aeronautical Engineering Division - IEA-E, Technological Institute of Aeronautics - ITA, Praça Marechal Eduardo Gomes, 50, Vila das Acácias, 12228-900, São José dos Campos, São Paulo, Brazil
donadon@ita.br

Abstract. *The peridynamic theory is a method for the numerical solution of the elastodynamics problems developed in recent years. One of its greatest advantages is the natural ability to simulate the initiation and growth of cracks in solid materials, without additional numerical procedures commonly employed in conventional finite element formulations. This ability is because the peridynamic constitutive relations are based on partial integral equations rather than differential ones, which are definite in a geometrical discontinuity. These constitutive relations are dependent on some constants calibrated by the physical and geometrical properties of the simulated problem, called in this work as the peridynamic material parameters. Within this context, this research aims to reevaluate these material parameters found in the open literature, to optimize computational costs and improve precision while running a peridynamic elastoplastic numerical analysis. To verify the improvements brought by the proposed methodology, these material parameters are implemented in an in-house elastoplastic peridynamic FORTRAN code, and the results for the displacements and the Von Mises stress fields are compared to the available analytical results and with those obtained with a commercial finite element code.*

Keywords: *Peridynamic Theory, Stress Analysis, Elastoplastic Simulations, Material Parameters*

1. INTRODUCTION

The Peridynamic Theory is a meshless method developed in the last years for the numerical solution of the elastodynamics problems. In a numerical simulation, the domain is represented by a cloud of points, which each point represents a small fraction of this domain. These points interact only with others that are within a maximum distance, called horizon (Bobaru *et al.*, 2017). This method has, among other advantages, a natural capacity to initiate and simulate the crack growth without additional numerical procedures, commonly employed in conventional finite elements formulations (Sarego *et al.*, 2016).

This advantage is due to the method being a nonlocal extension of continuum mechanics, where the balance of linear momentum is formulated as an integral equation, rather than a differential one. With this approach, the peridynamic constitutive equations continue to be valid with any geometrical discontinuity in numerical analysis, such as a crack (Bobaru *et al.*, 2017).

These constitutive equations are dependent on some constants, calibrated by the physical and geometrical properties of the simulated problem, named in this paper as the peridynamic material parameters (Madenci and Oterkus, 2014). Some approaches for calculating these constants are available in the open literature, in the work of Madenci and Oterkus (2014), Madenci and Oterkus (2016), and Pashazad and Kharazi (2019), for example.

These analytical parameters are obtained considering the entire region defined by a horizon, called neighborhood, to be completely embedded in the simulated material, which is not true near a free surface, as shown in Figure 1 (Madenci and Oterkus, 2014). If the same parameters from a complete neighborhood are used in these areas, the peridynamic constitutive relations behave slightly differently from this complete region. This difference is called the peridynamic surface effect (Le and Bobaru, 2018b). Furthermore, all points should have their volume inside this neighborhood, which is not true for points near this region's border (Madenci and Oterkus, 2014).

One way to minimize this surface effect is the calculation of the surface correction factor, as proposed in the literature (Le and Bobaru, 2018b). For the volume, a volume correction factor is also proposed for points near the neighborhood frontier (Madenci and Oterkus, 2014). Both correction factors need a considerable amount of floating-point operations to be used in a numerical analysis, which increases the computational effort.

Within this context, this research aims to reevaluate these material parameters found in the open literature to optimize computational costs and improve precision. To reach the objectives, these constants are calculated by a numerical approximation combined with a least square approach. These alternative methods eliminate the need to calculate any correction factor because they are already embedded in these numerical parameters.

To verify the improvements brought by the proposed methodology, these numerical material parameters are implemented into an in-house elastoplastic peridynamic FORTRAN code. The results obtained for the displacements and Von Mises stress field are compared to the available analytical results, previous version of the same FORTRAN code based on the classical approach available in the literature, and those obtained with a commercial finite element code.

2. THE PERIDYNAMIC THEORY

The peridynamic formulation used in this research is presented in Madenci and Oterkus (2014) and Madenci and Oterkus (2016). This ordinary state-based model is used, even with some limitations as small strains and infinitesimal rotations (Le and Bobaru, 2018a), due to its well-developed plasticity model with isotropic hardening (Madenci and Oterkus, 2016).

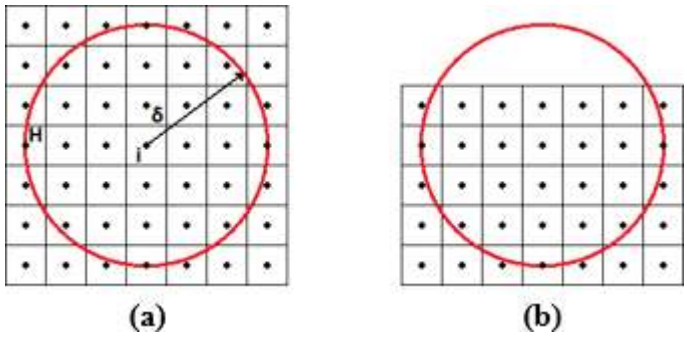

Figure 1. System of material points: (a) a complete neighborhood and (b) a neighborhood close to a free surface.

For a domain with equally spaced points by a distance Δ, as shown in Figure 1, where each point represents a volume V, the equation of motion for a single point i can be written by Eq. (1), where ρ_i is the mass density, $\ddot{\boldsymbol{u}}$ is the acceleration and **b** is the body force density vector. This point i is also the center of his neighborhood H, defined by the horizon δ, which contains N points j inside this area (Madenci and Oterkus, 2014). In this paper, the horizon δ is defined as three times the distance Δ (Bobaru *et al.*, 2017).

$$\rho_i \ddot{\boldsymbol{u}} = \sum_{j \in H} (\boldsymbol{t}_{ij} - \boldsymbol{t}_{ji}) V_j + \boldsymbol{b}_i, \tag{1}$$

The force state vector $\mathbf{t}_{ij}$ is defined in Eq. (2), where a_G, b, and d are three of the four peridynamic material constants that are covered in Section 3 (Madenci and Oterkus, 2016), and **x** and **y** are the distance vectors in the non-deformed and deformed configuration, respectively. The value of parameter a_k is given in Pashazad and Kharazi (2019).

$$\boldsymbol{t}_{ij} = \left[(a_k - a_G) 2\delta d \frac{\Lambda_{ij}}{|\boldsymbol{x}_j - \boldsymbol{x}_i|} \theta_i^e + 2\delta b s_{ij}^e \right] \frac{\boldsymbol{y}_j - \boldsymbol{y}_i}{|\boldsymbol{y}_j - \boldsymbol{y}_i|}, \tag{2}$$

The elastic dilatation θ_i^e, elastic stretch s_{ij}^e and the parameter Λ_{ij} are defined in Eq. (3) (Madenci and Oterkus, 2016).

$$\begin{aligned} \theta_i^e &= d\delta \sum_{j \in H} s_{ij}^e \Lambda_{ij} V_j \\ s_{ij}^e &= \frac{|\boldsymbol{x}_j - \boldsymbol{x}_i| - |\boldsymbol{y}_j - \boldsymbol{y}_i|}{|\boldsymbol{x}_j - \boldsymbol{x}_i|} - s_{ij}^{pl} \\ \Lambda_{ij} &= \frac{\boldsymbol{x}_j - \boldsymbol{x}_i}{|\boldsymbol{x}_j - \boldsymbol{x}_i|} \cdot \frac{\boldsymbol{y}_j - \boldsymbol{y}_i}{|\boldsymbol{y}_j - \boldsymbol{y}_i|} \end{aligned}, \tag{3}$$

The peridynamic strain energy density W_i and its dilatational W_i^k and distortional W_i^G components are given in Eq. (4) (Madenci and Oterkus, 2016).

$$W_i = W_i^k + W_i^G = \left(a_k \theta_i^{e\,2} \right) + \left(b\delta \sum_{j \in H} s_{ij}^{e\,2} |\boldsymbol{x}_j - \boldsymbol{x}_i| V_j - a_G \theta_i^{e\,2} \right), \tag{4}$$

The plastic stretch s_{ij}^{pl}, shown in Eq. (3), is calculated by the plasticity correction methodology presented by Madenci and Oterkus (2016) and Pashazad and Kharazi (2019). For a given time step, if the loading condition in any point surpass the yield surface, verified by the yield function F_i in Eq. (5) being greater than zero (Madenci and Oterkus, 2016), the plasticity effect needs to be corrected.

$$F_i = W_i^G - \frac{\left(\sigma_0 + E_t s_i^{pl}\right)^2}{6G}, \tag{5}$$

In Eq. (5), E_t is the tangent modulus, G is the shear modulus and σ_0 is the yield stress of the material. For a given time step n, the equivalent plastic stretch s_i^{pl} could be calculated by Eq. (6) (Madenci and Oterkus, 2016), where C_i is a positive proportionality constant and a_0 is the last material parameters reevaluated in this research.

$$s_i^{pl} = \left(s_i^{pl}\right)^{n-1} + C_i a_0 \sqrt{b\delta \sum_{j\in H} B_{ij}^2 |\boldsymbol{x}_j - \boldsymbol{x}_i| V_j}, \tag{6}$$

The value of the function B_{ij} is given in Eq. (7) (Pashazad and Kharazi, 2019).

$$B_{ij} = \left(s_{ij}^e\right)^{n-1} |\boldsymbol{x}_j - \boldsymbol{x}_i|, \tag{7}$$

Likewise, the plastic stretch s_{ij}^{pl} could be calculated by Eq. (8) (Madenci and Oterkus, 2016).

$$s_{ij}^{pl} = \left(s_{ij}^{pl}\right)^{n-1} + C_i B_{ij}, \tag{8}$$

In Madenci and Oterkus (2016) and Pashazad and Kharazi (2019), the value of the constant C_i is obtained using the Newton-Raphson iterative method on Eq. (5), with Eq. (6) and Eq. (8). However, substituting Eq. (6) and Eq. (8) into Eq. (5), and reorganizing the remaining expression leaving C_i in evidence, is possible to verify that this expression is a quadratic polynomial function of C_i, shown in Eq. (9).

$$\begin{aligned} F_i = {} & C_i^2 \left[b\delta \sum_{j\in H} B_{ij}^2 |\boldsymbol{x}_j - \boldsymbol{x}_i| V_j - a_G \left(d\delta \sum_{j\in H} B_{ij} \Lambda_{ij} V_j\right)^2 - \frac{\left(E_t a_0 \sqrt{b\delta \sum_{j\in H} B_{ij}^2 |\boldsymbol{x}_j - \boldsymbol{x}_i| V_j}\right)^2}{6G} \right] \\ & + C_i \left[2a_G d\delta (\theta_i^e)^{n-1} \sum_{j\in H} B_{ij} \Lambda_{ij} V_j - 2b\delta \sum_{j\in H} B_{ij}^2 V_j - \frac{E_t a_0 \sqrt{b\delta \sum_{j\in H} B_{ij}^2 |\boldsymbol{x}_j - \boldsymbol{x}_i| V_j} \left(\sigma_0 + E_t \left(s_i^{pl}\right)^{n-1}\right)}{3G} \right], \\ & + \left[b\delta \sum_{j\in H} B_{ij} \left(s_{ij}^e\right)^{n-1} V_j - a_G \left(\theta_i^{e2}\right)^{n-1} - \frac{\left(\sigma_0 + E_t \left(s_i^{pl}\right)^{n-1}\right)^2}{6G} \right] \end{aligned} \tag{9}$$

Analyzing the Eq. (9) is verified that the loading condition in a point surpasses the yield surface if the independent variable of this polynomial expression is greater than zero, and the value of C_i is then calculated as the lowest root from this equation. This definition agrees with the calculation based on the Newton-Raphson method proposed by Madenci and Oterkus (2016) and Pashazad and Kharazi (2019) because this method searches for the closest root of any equation from an initial seed, which is zero. This polynomial approach also helps to improve precision and decreases the simulation time, by obtaining the C_i through an analytical solution rather than a numerical approximation.

3. THE NEW APPROACH FOR THE MATERIAL PARAMETERS COMPUTATION

As cited in the Introduction, in this research the material parameters a_G, b, d, and a_0 will be calculated by a numerical analysis rather than by the analytical approach presented by Madenci and Oterkus (2014) and Madenci and Oterkus (2016). These new parameters are covered in the next sections.

3.1 Material Parameter d

The parameter d is calculated in Madenci and Oterkus (2014) by imposing an isotropic expansion loading condition on a fictitious complete neighborhood and solving the dilatation θ in Eq. (3) for d. In this proposed approach, the strain fields in Eq. (10) are imposed to the entire simulated domain, where ν is the Poisson ratio and the subscribes x, y, and z stands for the X-axis, Y-axis, and Z-axis direction, respectively.

$$\begin{aligned} &First\ loading\ condition: \varepsilon_x = \varepsilon;\ \varepsilon_y = \varepsilon_z = -\nu\varepsilon;\ \gamma_{xy} = \gamma_{xz} = \gamma_{yz} = 0 \\ &Second\ loading\ condition: \varepsilon_y = \varepsilon;\ \varepsilon_x = \varepsilon_z = -\nu\varepsilon;\ \gamma_{xy} = \gamma_{xz} = \gamma_{yz} = 0, \\ &Third\ loading\ condition: \varepsilon_z = \varepsilon;\ \varepsilon_x = \varepsilon_y = -\nu\varepsilon;\ \gamma_{xy} = \gamma_{xz} = \gamma_{yz} = 0 \end{aligned} \tag{10}$$

For a 3D analysis, applying these fields on Eq. (3) creates a system with three equations and only one variable (two equations for plane elasticity). These equations for point i are shown in Eq. (11), where the subscript n is the loading condition, and the dilatation θ for 3D and plane elasticity are given in Madenci and Oterkus (2014).

$$\begin{aligned} &For\ 3D: \left\{\delta \textstyle\sum_{j\in H} s_{ij}\Lambda_{ij}V_j\right\}_n \{d\} = \{\theta_i\}_n = \left\{\varepsilon_x + \varepsilon_y + \varepsilon_z\right\}_n = \{\varepsilon(1-2\nu)\}_n \\ &For\ plane\ elasticity: \left\{\delta \textstyle\sum_{j\in H} s_{ij}\Lambda_{ij}V_j\right\}_n \{d\} = \{\theta_i\}_n = \left\{\varepsilon_x + \varepsilon_y\right\}_n = \{\varepsilon(1-\nu)\}_n \end{aligned}, \tag{11}$$

The least square fitting method is used to obtain the best fit for d to all equations in this overdetermined linear system. If only one loading condition is used to solve the value of d, the parameter could be driven by this loading condition. Considering Eq. (11), the best fit for d is the solution of the linear system in Eq. (12) (Weisstein, 2002), where $[a]$ is the system's matrix, $\{x\}$ is variable vector, and $\{y\}$ is the solution vector.

$$[a]^T[a]\{x\} = [a]^T\{y\}, \tag{12}$$

3.2 Material Parameter a_G and b

The parameters a_G and b are related by the strain energy density equation in Eq. (4). For these two variables to be computed together, at least another extra equation is required. Both are also related by the equation of motion in Eq. (1) with the force state vector in Eq. (2), but for the imposed strain fields its value is zero for any direction, creating an underdetermined system of equation. To overcome this problem, a new set of equations are also proposed here.

For local interactions, Madenci and Oterkus (2014) proposed an approximation for the stress field based on the force state vector, which could be used in this proposed approach. However, these stress equations need to be redeveloped for a non-local interaction, especially because the material parameters for a local interaction are different from the non-local ones due to the length of the horizon for these two approaches.

For a continuum mechanics approach, the equation of motion can be expressed by the stress components, as shown in Eq. (13) (Madenci and Oterkus, 2014).

$$\begin{aligned} \rho_i \ddot{u}_{x\,i} &= \sigma_{xx,x\,i} + \sigma_{xy,y\,i} + \sigma_{xz,z\,i} + b_{x\,i} \\ \rho_i \ddot{u}_{y\,i} &= \sigma_{yx,x\,i} + \sigma_{yy,y\,i} + \sigma_{yz,z\,i} + b_{y\,i}, \\ \rho_i \ddot{u}_{z\,i} &= \sigma_{zx,x\,i} + \sigma_{zy,y\,i} + \sigma_{zz,z\,i} + b_{z\,i} \end{aligned} \tag{13}$$

Likewise done by Madenci and Oterkus (2014) the Eq. (13) are approximated by the finite difference method. In this research, the backward difference method is used on Eq. (13) to approximate the stress components, where each component is calculated by an average of each finite difference from point i to all N points j inside his neighborhood. For brevity, only the first difference is shown in Eq. (14), also Δ_x, Δ_y, and Δ_z are the distance between points i and j on the non-deformed configuration on X-axis, Y-axis, and Z-axis respectively.

$$\begin{aligned} \rho_i \ddot{u}_{x\,i} &= \frac{1}{N}\frac{(\sigma_{xx\,i} - \sigma_{xx\,j})}{\Delta_x} + \cdots + \frac{1}{N}\frac{(\sigma_{xy\,i} - \sigma_{xy\,j})}{\Delta_y} + \cdots + \frac{1}{N}\frac{(\sigma_{xz\,i} - \sigma_{xz\,j})}{\Delta_z} + \cdots + b_{x\,i} \\ \rho_i \ddot{u}_{y\,i} &= \frac{1}{N}\frac{(\sigma_{yx\,i} - \sigma_{yx\,j})}{\Delta_x} + \cdots + \frac{1}{N}\frac{(\sigma_{yy\,i} - \sigma_{yy\,j})}{\Delta_y} + \cdots + \frac{1}{N}\frac{(\sigma_{yz\,i} - \sigma_{yz\,j})}{\Delta_z} + \cdots + b_{y\,i}, \\ \rho_i \ddot{u}_{z\,i} &= \frac{1}{N}\frac{(\sigma_{zx\,i} - \sigma_{zx\,j})}{\Delta_x} + \cdots + \frac{1}{N}\frac{(\sigma_{zy\,i} - \sigma_{zy\,j})}{\Delta_y} + \cdots + \frac{1}{N}\frac{(\sigma_{zz\,i} - \sigma_{zz\,j})}{\Delta_z} + \cdots + b_{z\,i} \end{aligned} \tag{14}$$

Setting each term of Eq. (14) equal to those in Eq. (1) with Eq. (2), and reorganizing the expressions in the same way as done by Madenci and Oterkus (2014) in their local interaction approach, one of the possible ways to approximate the stress fields for this non-local approach is shown in Eq. (15).

$$\sigma_{xx\,i} = \sum_{j\in H} \frac{t_{ij}\Delta_x (y_j - y_i)_x V_j}{|y_j - y_i|} \;;\; \sigma_{xy\,i} = \sum_{j\in H} \frac{t_{ij}\Delta_y (y_j - y_i)_x V_j}{|y_j - y_i|} \;;\; \sigma_{xz\,i} = \sum_{j\in H} \frac{t_{ij}\Delta_z (y_j - y_i)_x V_j}{|y_j - y_i|}$$
$$\sigma_{yx\,i} = \sum_{j\in H} \frac{t_{ij}\Delta_x (y_j - y_i)_y V_j}{|y_j - y_i|} \;;\; \sigma_{yy\,i} = \sum_{j\in H} \frac{t_{ij}\Delta_y (y_j - y_i)_y V_j}{|y_j - y_i|} \;;\; \sigma_{yz\,i} = \sum_{j\in H} \frac{t_{ij}\Delta_z (y_j - y_i)_y V_j}{|y_j - y_i|}, \tag{15}$$
$$\sigma_{zx\,i} = \sum_{j\in H} \frac{t_{ij}\Delta_x (y_j - y_i)_z V_j}{|y_j - y_i|} \;;\; \sigma_{zy\,i} = \sum_{j\in H} \frac{t_{ij}\Delta_y (y_j - y_i)_z V_j}{|y_j - y_i|} \;;\; \sigma_{zz\,i} = \sum_{j\in H} \frac{t_{ij}\Delta_z (y_j - y_i)_z V_j}{|y_j - y_i|}$$

To avoid any inconsistencies when calculating the shears stresses from Eq. (15), as their values could be different when calculating from X-axis, Y-axis, and Z-axis, these shear stresses are evaluated by their averages. So, the stress fields are calculated as shown in Eq. (16).

$$\sigma_{xx\,i} = \sum_{j\in H} \frac{t_{ij}(x_j - x_i)_x (y_j - y_i)_x V_j}{|y_j - y_i|} \;;\; \sigma_{yy\,i} = \sum_{j\in H} \frac{t_{ij}(x_j - x_i)_y (y_j - y_i)_y V_j}{|y_j - y_i|} \;;\; \sigma_{zz\,i} = \sum_{j\in H} \frac{t_{ij}(x_j - x_i)_z (y_j - y_i)_z V_j}{|y_j - y_i|}$$
$$\sigma_{xy\,i} = \sum_{j\in H} \frac{t_{ij}\left[(x_j - x_i)_y (y_j - y_i)_x + (x_j - x_i)_x (y_j - y_i)_y\right] V_j}{2|y_j - y_i|} \;;\; \sigma_{xz\,i} = \sum_{j\in H} \frac{t_{ij}\left[(x_j - x_i)_z (y_j - y_i)_x + (x_j - x_i)_x (y_j - y_i)_z\right] V_j}{2|y_j - y_i|}, \tag{16}$$
$$\sigma_{yz\,i} = \sum_{j\in H} \frac{t_{ij}\left[(x_j - x_i)_z (y_j - y_i)_y + (x_j - x_i)_y (y_j - y_i)_z\right] V_j}{2|y_j - y_i|}$$

The loading condition in Eq. (10) returns a uniaxial stress field in the simulated domain. Using the normal stresses from Eq. (16), and substituting the state force t_{ij} (Madenci and Oterkus, 2016) onto this equation, is possible then to calculate the values of a_G and b with an overdetermined system of equation.

For a 3D analysis, applying these definitions creates a system with nine equations and two variables. As for a plane stress analysis, these equations also create a system of four equations and two variables. For brevity, these equations for a single loading condition are shown in Eq. (17).

$$For\ 3D: \begin{bmatrix} \sum_{j\in H} \frac{2\delta d \Lambda_{ij} \theta_i (x_j - x_i)_x (y_j - y_i)_x V_j}{|\boldsymbol{x_j} - \boldsymbol{x_i}||y_j - y_i|} & \sum_{j\in H} \frac{2\delta s_{ij} (x_j - x_i)_x (y_j - y_i)_x V_j}{|\boldsymbol{x_j} - \boldsymbol{x_i}||y_j - y_i|} \\ \sum_{j\in H} \frac{2\delta d \Lambda_{ij} \theta_i (x_j - x_i)_y (y_j - y_i)_y V_j}{|\boldsymbol{x_j} - \boldsymbol{x_i}||y_j - y_i|} & \sum_{j\in H} \frac{2\delta s_{ij} (x_j - x_i)_y (y_j - y_i)_y V_j}{|\boldsymbol{x_j} - \boldsymbol{x_i}||y_j - y_i|} \\ \sum_{j\in H} \frac{2\delta d \Lambda_{ij} \theta_i (x_j - x_i)_z (y_j - y_i)_z V_j}{|\boldsymbol{x_j} - \boldsymbol{x_i}||y_j - y_i|} & \sum_{j\in H} \frac{2\delta s_{ij} (x_j - x_i)_z (y_j - y_i)_z V_j}{|\boldsymbol{x_j} - \boldsymbol{x_i}||y_j - y_i|} \end{bmatrix}_n \begin{Bmatrix} a_k - a_G \\ b \end{Bmatrix} = \begin{Bmatrix} \sigma_{xx\,n} \\ \sigma_{yy\,n} \\ \sigma_{zz\,n} \end{Bmatrix}_n,$$
$$For\ plane\ elasticity: \begin{bmatrix} \sum_{j\in H} \frac{2\delta d \Lambda_{ij} \theta_i (x_j - x_i)_x (y_j - y_i)_x V_j}{|\boldsymbol{x_j} - \boldsymbol{x_i}||y_j - y_i|} & \sum_{j\in H} \frac{2\delta s_{ij} (x_j - x_i)_x (y_j - y_i)_x V_j}{|\boldsymbol{x_j} - \boldsymbol{x_i}||y_j - y_i|} \\ \sum_{j\in H} \frac{2\delta d \Lambda_{ij} \theta_i (x_j - x_i)_y (y_j - y_i)_y V_j}{|\boldsymbol{x_j} - \boldsymbol{x_i}||y_j - y_i|} & \sum_{j\in H} \frac{2\delta s_{ij} (x_j - x_i)_y (y_j - y_i)_y V_j}{|\boldsymbol{x_j} - \boldsymbol{x_i}||y_j - y_i|} \end{bmatrix}_n \begin{Bmatrix} a_k - a_G \\ b \end{Bmatrix} = \begin{Bmatrix} \sigma_{xx\,n} \\ \sigma_{yy\,n} \end{Bmatrix}_n \tag{17}$$

These systems are solved as shown in Eq. (12). However, these systems give the parameter b and the subtraction of a_k and a_G. Using the value of a_k given by Pashazad and Kharazi (2019), the parameter a_G can be easily obtained.

3.3 Material Parameter a_0

The parameter a_0 is calculated in Madenci and Oterkus (2016) by imposing a uniaxial loading condition with zero dilatation on X-axis. This loading is applied on a fictitious complete neighborhood, and Eq. (18) is then used to calculate this parameter, where $\Delta\zeta$ is the imposed incremental plastic stretch. This zero dilatation condition arises due to the fictitious plastic deformation condition (Madenci and Oterkus, 2016).

$$a_0 = \frac{\Delta\zeta}{\sqrt{b\delta \sum_{j\in H} B_{ij}^2 |\boldsymbol{x_j} - \boldsymbol{x_i}| V_j}}, \tag{18}$$

The new approach to calculate a_0 is almost the same as shown in Section 3.1. The strain fields in Eq. (19) are imposed on the entire simulated domain to represent an incremental plastic loading.

$$First\ loading\ condition: \varepsilon_x = \Delta\zeta;\ \varepsilon_y = \varepsilon_z = -\frac{\Delta\zeta}{2};\ \gamma_{xy} = \gamma_{xz} = \gamma_{yz} = 0$$
$$Second\ loading\ condition: \varepsilon_y = \Delta\zeta;\ \varepsilon_x = \varepsilon_z = -\frac{\Delta\zeta}{2};\ \gamma_{xy} = \gamma_{xz} = \gamma_{yz} = 0, \tag{19}$$
$$Third\ loading\ condition: \varepsilon_z = \Delta\zeta;\ \varepsilon_x = \varepsilon_y = -\frac{\Delta\zeta}{2};\ \gamma_{xy} = \gamma_{xz} = \gamma_{yz} = 0$$

For a 3D analysis, applying these fields on Eq. (18) also creates a system with three equations and only one variable (two equations for plane elasticity), which are also solved by the least square fitting in Eq. (12). The equations for point i and both the 3D and plane analysis are shown in Eq. (20).

$$\left\{\sqrt{b\delta \sum_{j\in H} B_{ij}^2 |\boldsymbol{x}_j - \boldsymbol{x}_i| V_j}\right\}_n \{a_0\} = \{\Delta\zeta\}_n, \tag{20}$$

4. NUMERICAL RESULTS

In this paper, an in-house FORTRAN previously developed by the authors (Cruz and Donadon, 2019) was updated with all definitions and equations described herein. The time integration scheme used within this code is the adaptive dynamic relaxation method, where the weight function is the velocity vector on a half previous time step (Oakley and Knight Jr, 1995), and the stable time step is calculated by the Courant-Friedrichs-Lewy approach (Bobaru et al., 2017). The steady-state is achieved when the relative difference of the strain energy between two time steps is lower than 10^{-10}.

With these considerations, this code is used in three numerical tests aimed to verify the improvements brought by the present research. The first test compares the updated code's accuracy with the older code using the energy surface correction factor (Le and Bobaru, 2018b), a volume correction factor (Madenci and Oterkus, 2014), and the analytical material parameters (Pashazad and Kharazi, 2019). This accuracy is calculated with the closed-form solutions obtained from elasticity theory. The second test evaluates the shape of the stress-strain curve for a plate under loading and unloading in the plastic regime, observing the accuracy of the plastic corrections. In the third test, one plate has a hole and the other has a crack to evaluate the concentration of stresses when loaded in the plastic regime, as shown in Figure 2. This crack is treated in this paper as a free surface.

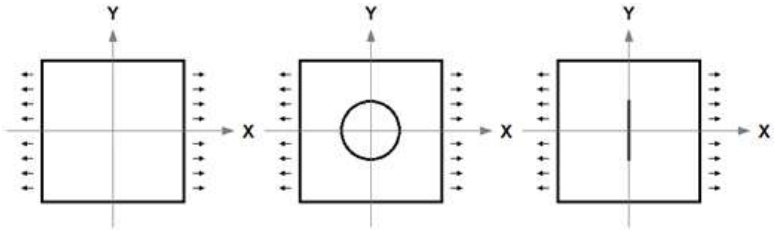

Figure 2. The simulated plates.

The mechanical and physical properties of this plate are Poisson´s ratio 0.342, density 4428kg/m³, yield stress 1.017GPa, Young modulus 113GPa, and tangent modulus 1.38GPa. The dimensions of the plate are length 1000mm, width 1000mm, thickness 1mm, a diameter of hole (2r) of 300mm, length of crack (2a) 300mm, and length of the boundary layer 60mm for the first and second test, and 15mm for the third test.

In the first and second test, the distance between points Δ is 10mm and for the third test is 2.5mm. For the first test, a strain of ε_x=5mm/m is imposed on the indicated edges in Figure 2. To avoid abrupt loading, this strain is applied incrementally with a factor of 1/1000 time steps. For the second test, a strain of ε_x=141mm/m is imposed with intermediate unloading down to ε_x=62.5mm/m from ε_x=68mm/m, and with a loading factor of 1/15000 time steps. Finally, in the third test, a displacement field of u_x=-4mm (left side) u_x=4mm (right side), and u_y=0m are applied, with a factor of 1/15000 time steps. For all tests, ε=Δζ=1mm/m in Eq. (10) and Eq. (19).

4.1 First Test (Plate Under Elastic Loading)

For this test, the errors for displacements on X direction for the proposed methodology and with a previous approach based on the classical volume and surface correction are shown in Figure 3.

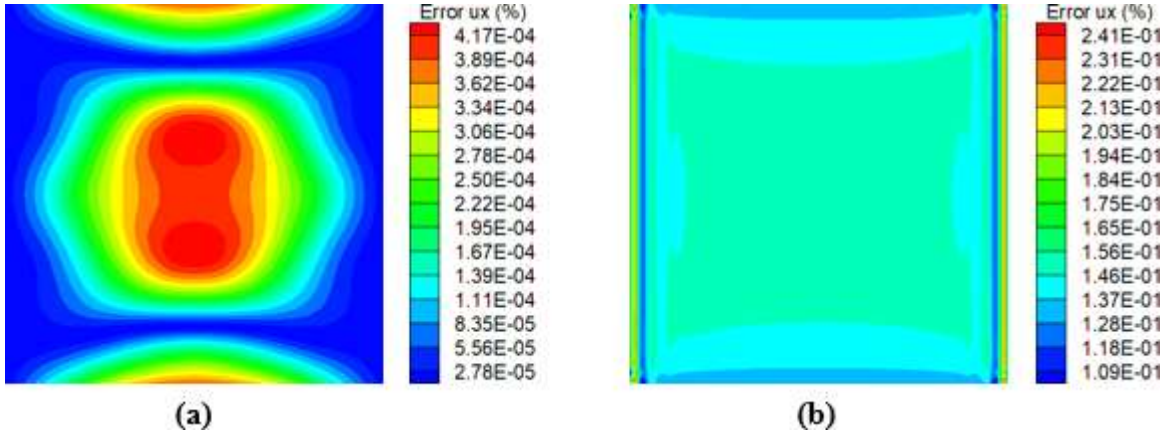

Figure 3. Displacement error field on X direction for: (a) proposed methodology and (b) classical volume and surface correction approach.

The error field for displacements on Y direction for the proposed methodology and the older approach is shown in Figure 4.

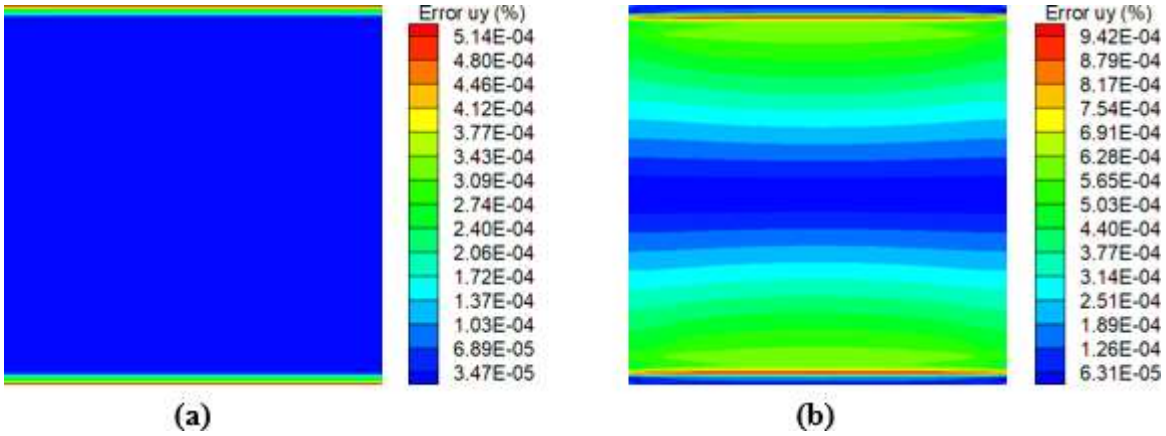

Figure 4. Displacement error field on Y direction for: (a) proposed methodology and (b) classical volume and surface correction approach.

Analyzing Figure 3 and Figure 4 is clear that the results for the displacements for the updated code are much closer to the analytical ones than those obtained with the approach found in the literature. For the updated program, the maximum error in the displacements in the X-axis direction is 0.0004457%, while the average error is 0.000163%. For the displacements in the Y-axis direction, the maximum error is 0.000549%, while the average error is 0.000037%. For the classical volume and surface correction approach, the maximum error in the displacements in the X-axis direction is 0.250397%, while the average error is 0.147294%. For the displacements in the Y-axis direction, the maximum error is 0.001005%, while the average error is 0.000314%.

The updated code simulated this test in 36.641sec, while the older code processed in 49.672sec. This large reduction in processing time is due to the smaller amount of floating-point operations required in the proposed approach since the correction factors of the older code are already integrated into the peridynamic parameters of the updated code.

4.2 Second Test (Plate Under Plastic Loading)

For the most central point, the equivalent stress by the equivalent plastic stretch s_i^{pl} is given in Figure 5 for two situations: an uninterrupted loading condition and a loading with intermediary unload condition. The Von Mises equivalent stress $\sigma_{VM\,i}$ used in this paper is obtained by Eq. (21) (Madenci and Oterkus, 2016).

$$\sigma_{VM\,i} = \sqrt{6GW_i^G}, \tag{21}$$

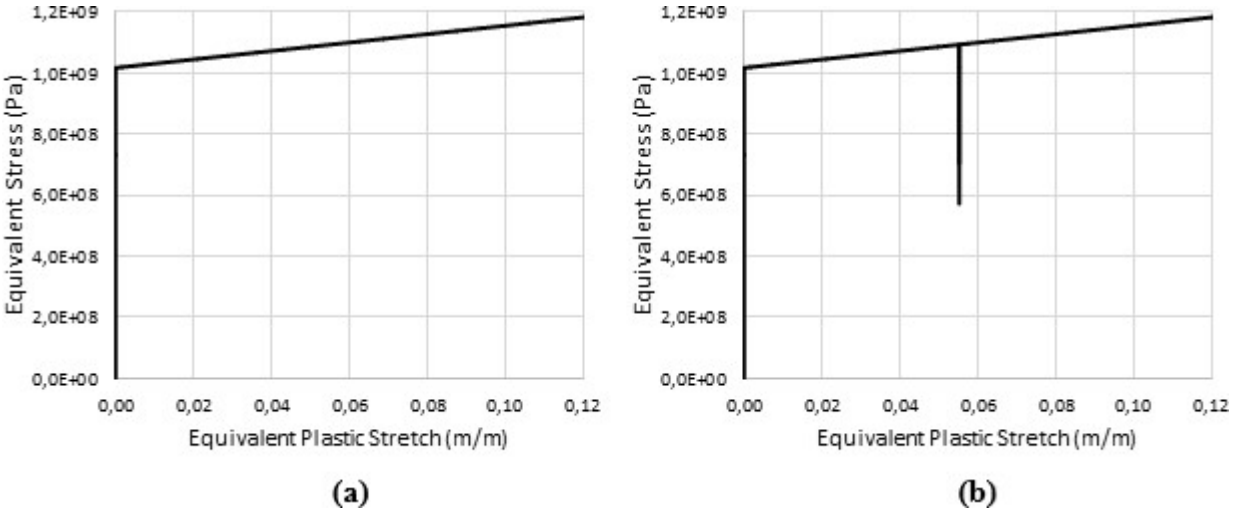

Figure 5. Equivalent stress by equivalent plastic stretch for: (a) uninterrupted loading and (b) loading with unloading.

The results in Figure 5 are very close to those expected. The tangent modulus returned by both loading condition is exactly the prescribed, which means no oscillations was found in the plastic regimen in this test. The yield starts in the predicted region, and the unloading process occurred as expected, with the hardening resuming in the exact spot where stopped. This result agrees with those from Section 4.1, showing the accuracy of the proposed methodology.

4.3 Third Test (Plate With Discontinuity)

In the final test, the Von Mises stress field obtained by the updated code is compared by the same field obtained by the Abaqus FE code, where the geometry and the loading conditions force the simulated plate to exhibit a mixed elastic/plastic behavior. The FE model is developed using CPS3 elements, combined with an elastoplastic constitutive model available in the Abaqus material library. For a plate with a central hole, the equivalent stress fields are depicted in Figure 6.

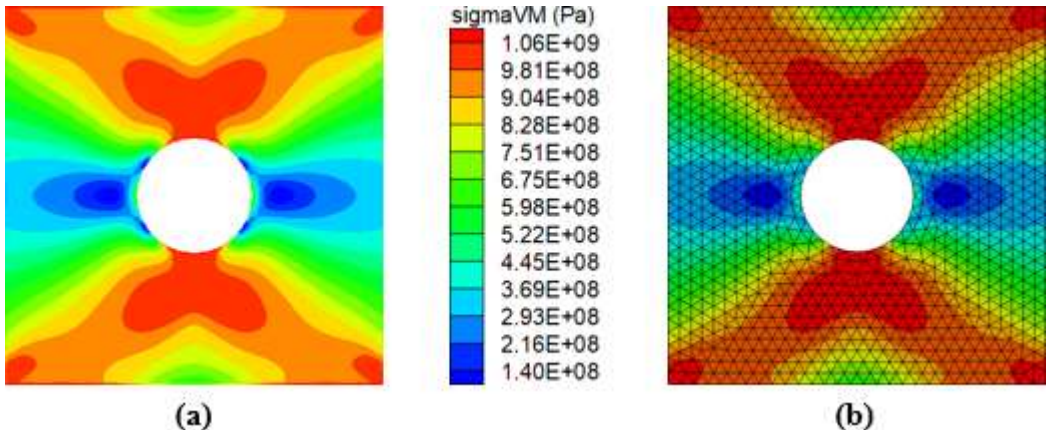

Figure 6. Von Mises stress field for: (a) updated in-house FORTRAN code and (b) Abaqus.

For a plate with a central crack, the equivalent stress fields are depicted in Figure 7.

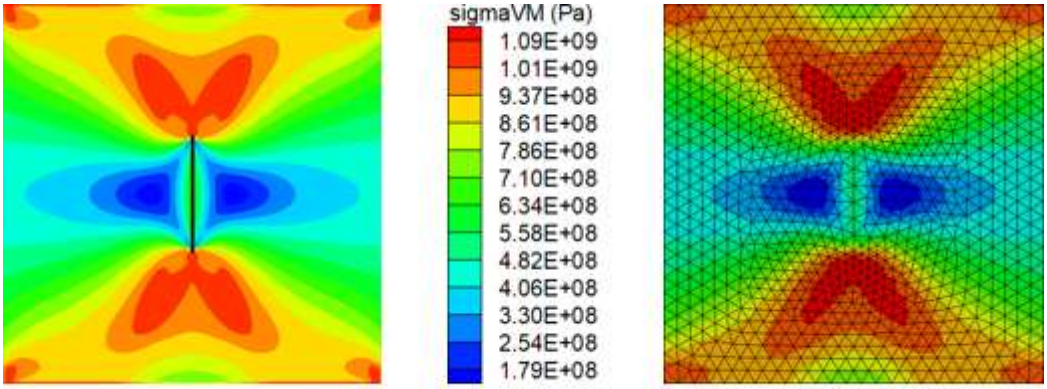

Figure 7. Von Mises stress field for: (a) in-house FORTRAN code and (b) Abaqus.

As shown in Figure 6 and Figure 7, the results obtained through the peridynamic proposed approach are very close to those obtained by the finite element simulations, which is expected by the results from the two previous tests.

5. CONCLUSIONS

This paper presented an alternative approach for calculating the peridynamic material parameters embedded with the surface and volume correction factors. The new approach was implemented into an in-house FORTRAN-based code and some validation cases were presented and discussed. The proposed approach has significantly improved the accuracy of results and led to significant reductions in computational time when compared to the classical volume/surface correction approach. With these new sets of parameters, the results brought by the in-house FORTRAN are very competitive compared with the FE code predictions, and much better in terms of accuracy than those previously presented by the authors (Cruz and Donadon, 2019).

6. ACKNOWLEDGEMENTS

This project is partially funded by CNPq, grant number 301053/2016-2.

7. REFERENCES

Bobaru, F., Foster, J.T., Geubelle, P.H., Silling, S.A., 2016. *Advances in Applied Mathematics: Handbook of Peridynamic Modeling*. Editora CRC Press, New York.

Cruz, A.L., Donadon, M.V., 2019, "Application of the Peridynamic Theory in the Stress Field Analysis of Plates with Geometric Discontinuities". In *Proceedings of 7th International Symposium on Solid Mechanics - MECSOL 2019*. São Carlos, Brazil.

Le, Q.V., Bobaru, F., 2018a, "Objectivity of State-Based Peridynamic Models for Elasticity", *Journal of Elasticity*, Vol. 131, No. 1, pp. 1-17.

Le, Q.V., Bobaru, F., 2018b, "Surface Corrections for Peridynamic Models in Elasticity and Fracture", *Computational Mechanics*. Vol. 61, No. 4, pp. 499-518.

Madenci, E., Oterkus, E., 2014. *Peridynamic Theory and Its Applications*. Editora Springer, New York.

Madenci, E., Oterkus, S., 2016, "Ordinary State-based Peridynamics for Plastic Deformation According to Von Mises Yield Criteria with Isotropic Hardening", *Journal of the Mechanics and Physics of Solids*. Vol. 86, No. 1, pp. 192-219.

Oakley, D.R., Knight Jr, N.F., 1995, "Adaptive Dynamic Relaxation Algorithm for Non-linear Hyperelastic Structures: Part I Formulation", *Computer Methods in Applied Mechanics and Engineering*, Vol. 126, No. 1-2, pp. 67-89.

Pashazad, H., Kharazi, M., 2019, "A Peridynamic Plastic Model Based on Von Mises Criteria with Isotropic, Kinematic and Mixed Hardenings under Cyclic Loading", *International Journal of Mechanical Sciences*, Vol. 156, No. 1, pp. 182-204.

Sarego, G., Le, Q.V., Bobaru, F., Zaccariotto, M., Galvanetto, U., 2016, "Linearized State-based Peridynamics for 2-D Problems", *International Journal for Numerical Methods in Engineering*, Vol. 108, No. 10, pp. 1174-1197.

Weisstein, E.W., 2002. *CRC Concise Encyclopedia of Mathematics, Second Edition*. Editora Chapman and Hall/CRC, Boca Raton.

8. RESPONSIBILITY NOTICE

The authors are the only responsible for the printed material included in this paper.